

Appendix A: Lead isotope framework of northern Heilongjiang province and descriptions of the Au-Ag deposits for “Lead and noble gas isotopic constraints on the origin of Te-bearing adularia-sericite epithermal Au-Ag deposits in a calc-alkaline magmatic arc, NE China”

Shen Gao^{1, 2}, Albert H. Hofstra³, Kezhang Qin^{2, 4}, Xinyu Zou², Michael J. Pribil³, Andrew G. Hunt³, Andrew H. Manning³, Heather A. Lowers³, Hong Xu¹

¹ *School of Earth Sciences and Resources, China University of Geosciences (Beijing), Beijing 100083, China*

² *Key Laboratory of Mineral Resources, Institute of Geology and Geophysics, Chinese Academy of Sciences, Beijing 100029, China*

³ *U.S. Geological Survey, P.O. Box 25046, Denver, CO 80225, USA*

⁴ *University of Chinese Academy of Sciences, Beijing 100049, China*

Any use of trade, firm, or product names is for descriptive purposes only and does not imply endorsement by the U.S. Government.

Contents

1. Lead Isotope Framework of Northern Heilongjiang Province.
2. Descriptions of the Au-Ag Deposits.
3. Figs. A1–A3.

References

1. Lead Isotope Framework of Northern Heilongjiang Province

In northeastern China, the stratigraphy is complex and the lead isotope framework has not been well established. The lead isotope compositions of Cambrian to Cenozoic rocks in the study area are shown on Figure A1, and the lead isotope compositions of sulfides from the deposits are shown on Figure A2. Data are split into five groups of rocks as follows: (i) Cambrian metasedimentary basement; (ii) Ordovician igneous rocks related to subduction of the Paleo-Asian Ocean; (iii) Triassic to Jurassic igneous rocks related to subduction of the Mongolia-Okhotsk Ocean; (iv) Cretaceous igneous rocks related to subduction of the Paleo-Pacific Ocean; and (v) Cenozoic intraplate basalt. The following discussion of the rock sequences is based on Pb isotope evolution diagrams (Fig. A1a, b) and radiogenic Pb isotope diagrams (Fig. A1c, d).

1.1. Cambrian metasedimentary basement

Cambrian metasedimentary rocks have the highest range of $^{206}\text{Pb}/^{204}\text{Pb}$ values from 18.314 to 20.897 in the area (Appendix B Table B1 and Fig. A1a). One sample has a low $^{206}\text{Pb}/^{204}\text{Pb}$ value of 18.314, the others are higher than 19. Their $^{207}\text{Pb}/^{204}\text{Pb}$ values range from 15.617 to 15.916 and $^{208}\text{Pb}/^{204}\text{Pb}$ from 37.671 to 38.767 (Appendix B Table B1 and Fig. A1b). On the $^{208}\text{Pb}/^{204}\text{Pb}$ vs. $^{206}\text{Pb}/^{204}\text{Pb}$ diagram (Fig. A1b), Cambrian marble, slate, and biotite granite plot under and extend beyond the average crustal curve of Stacey and

Kramers (1975). These rocks have the most radiogenic Pb. Sulfides from a Cambrian skarn W deposit have a range of $^{206}\text{Pb}/^{204}\text{Pb}$ values that is similar to the basement (Appendix B Table B1 and Fig. A2a, b).

1.2. Ordovician igneous rocks

Ordovician granite porphyry, diorite, and andesitic tuff have a low $^{206}\text{Pb}/^{204}\text{Pb}$ range from 17.560 to 18.392 in the area (Appendix B Table B1 and Fig. A1a). These rocks have a range of $^{207}\text{Pb}/^{204}\text{Pb}$ values from 15.148 to 15.586 and $^{208}\text{Pb}/^{204}\text{Pb}$ from 36.617 to 37.707 (Appendix B Table B1 and Fig. A1b) and plot under the average crustal curve of Stacey and Kramers (1975) (Fig. A1a, b). These rocks have less radiogenic Pb, which may reflect partial melting of lower crust, and are related to Ordovician porphyry Cu-Au mineralization. Sulfides from Ordovician porphyry Cu-Au and intermediate sulfidation epithermal Au deposits have Pb isotope values that are similar to Ordovician igneous rocks (Appendix B Table B1 and Fig. A2a, b).

1.3. Triassic to Jurassic igneous rocks

Triassic diorite and monzogranite have $^{206}\text{Pb}/^{204}\text{Pb}$ values from 17.390 to 18.978, $^{207}\text{Pb}/^{204}\text{Pb}$ values from 15.357 to 15.621 and $^{208}\text{Pb}/^{204}\text{Pb}$ values from 37.230 to 38.498 (Appendix B Table B1 and Fig. A1a, b). Jurassic monzogranite, granodiorite, and volcanic

rocks have a similar range of $^{206}\text{Pb}/^{204}\text{Pb}$ values from 17.963 to 19.078. Jurassic rocks have $^{207}\text{Pb}/^{204}\text{Pb}$ values from 15.526 to 15.612 and $^{208}\text{Pb}/^{204}\text{Pb}$ values from 37.961 to 38.719 (Appendix B Table B1 and Fig. A1a, b). On the $^{207}\text{Pb}/^{204}\text{Pb}$ vs. $^{206}\text{Pb}/^{204}\text{Pb}$ diagram (Fig. A1a), the Triassic and Jurassic rocks plot under the average crustal curve of Stacey and Kramers (1975). These rocks have moderately radiogenic Pb, which may reflect partial melting of lower crust. Sulfides from porphyry Mo, orogenic Au, Te, and Sb, and skarn W, Mo, Zn, Fe, and Cu deposits overlap the range of contemporary igneous rocks (Appendix B Table B1 and Fig. A2a, b).

1.4. Cretaceous igneous rocks

Cretaceous andesite, dacite, granodiorite, granodioritic porphyry, granite porphyry, and tuff and have $^{206}\text{Pb}/^{204}\text{Pb}$ ratios from 17.679 to 18.758, $^{207}\text{Pb}/^{204}\text{Pb}$ ratios from 15.484 to 15.703 and $^{208}\text{Pb}/^{204}\text{Pb}$ ratios from 37.754 to 39.643 (Appendix B Table B1 and Fig. A1a, b). Cretaceous rocks overlap the average crustal curve of Stacey and Kramers (1975) and part of the range of Triassic and Jurassic igneous rocks on $^{207}\text{Pb}/^{204}\text{Pb}$ vs. $^{206}\text{Pb}/^{204}\text{Pb}$ and $^{208}\text{Pb}/^{204}\text{Pb}$ vs. $^{206}\text{Pb}/^{204}\text{Pb}$ diagrams (Fig. A1a, b). These rocks were generated by partial melting of the younger lower crust. Sulfides from coeval epithermal Au-Ag \pm Te deposits overlap the range of Cretaceous igneous rocks (Appendix B Table B1 and Fig. A2a, b).

1.5. Cenozoic potassic basalt

Cenozoic potassic basalt has the lowest range of $^{206}\text{Pb}/^{204}\text{Pb}$ values from 16.607 to 17.254, $^{207}\text{Pb}/^{204}\text{Pb}$ values from 15.352 to 15.482, and $^{208}\text{Pb}/^{204}\text{Pb}$ values from 36.511 to 37.312 (Appendix B Table B1 and Fig. 8a, b). On the $^{208}\text{Pb}/^{204}\text{Pb}$ vs. $^{206}\text{Pb}/^{204}\text{Pb}$ diagram (Fig. 4a), Cenozoic potassic basalt lies under the average crustal curve of Stacey and Kramers (1975), reflecting a mantle source.

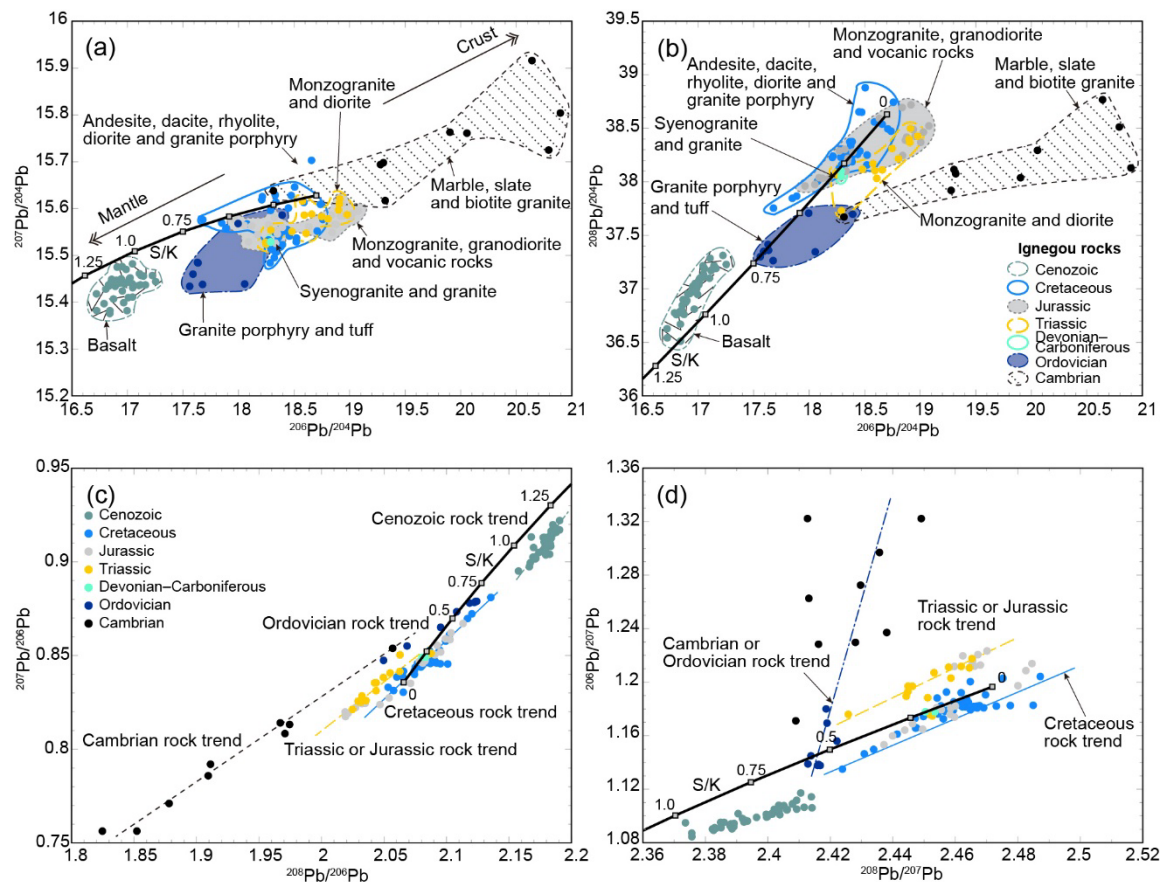


Fig. A1. Lead isotope compositions of Cambrian to Cenozoic metamorphic and igneous rocks in the north of Heilongjiang province, NE China. (a). $^{207}\text{Pb}/^{204}\text{Pb}$ versus $^{206}\text{Pb}/^{204}\text{Pb}$.

(b). $^{208}\text{Pb}/^{204}\text{Pb}$ versus $^{206}\text{Pb}/^{204}\text{Pb}$. (c). $^{206}\text{Pb}/^{207}\text{Pb}$ versus $^{208}\text{Pb}/^{207}\text{Pb}$. The Cambrian and Ordovician rock and Triassic and Jurassic rock contamination trends in this diagram are evident in Cretaceous igneous rocks. (d). $^{207}\text{Pb}/^{206}\text{Pb}$ versus $^{208}\text{Pb}/^{206}\text{Pb}$. The average crustal curve is from Stacey and Kramers (1975). (Data from Du 1985; Basu et al. 1991; Zhang et al. 1995, 2017; Zou et al. 2003; Han 2004, 2013; Wang et al. 2006b, 2016, 2017; Li 2011, 2018; Rasskazov et al. 2011; Zheng 2012; Zhang et al. 2014; Hao et al. 2016; Chen et al. 2017; Gao et al. 2017a, b, 2018; Deng et al. 2018; Zhai et al. 2018; Zhao et al. 2020).

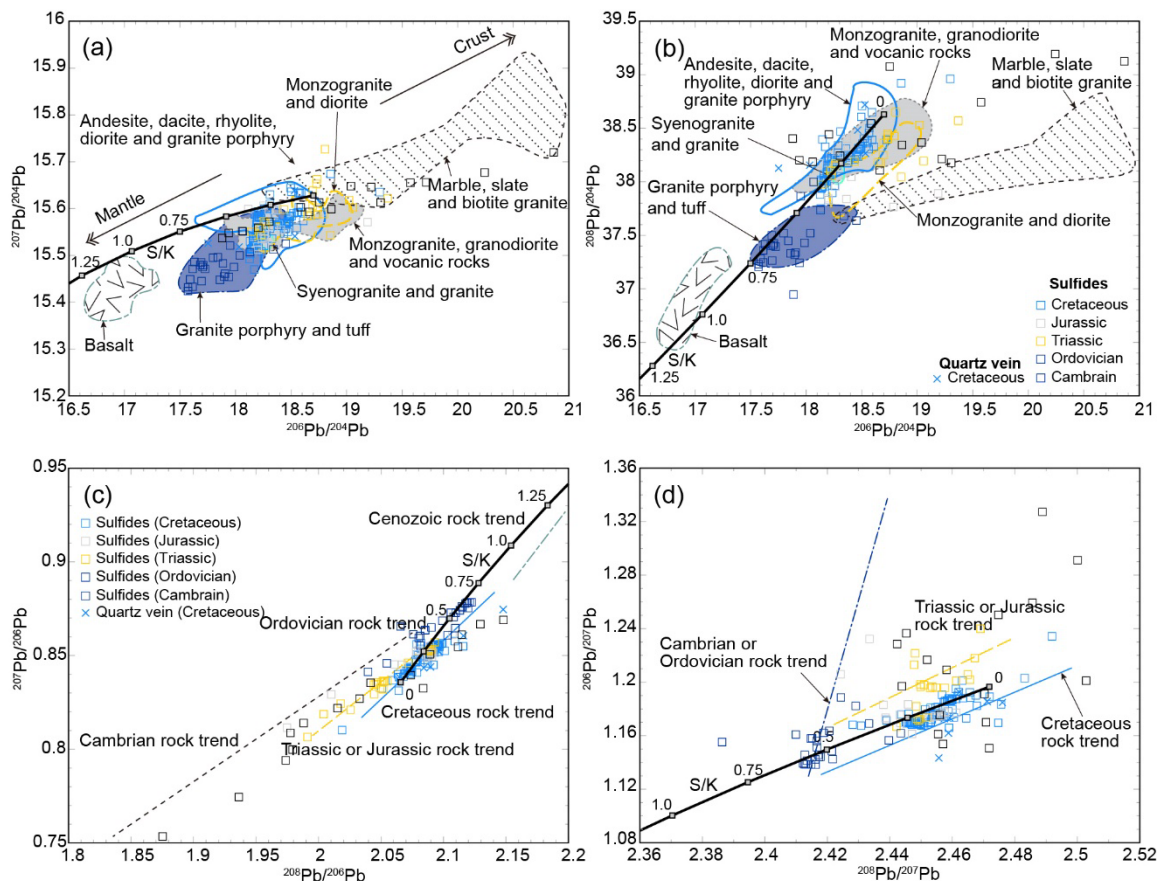


Fig. A2. Lead isotope compositions of sulfides (pyrrhotite, pyrite, chalcopyrite, galena,

molybdenite, and bornite) in Cretaceous epithermal deposits relative to the Cambrian, Ordovician, Triassic, Jurassic, Cretaceous, and Cenozoic rock trends in the north Heilongjiang province, NE China. (a). $^{207}\text{Pb}/^{204}\text{Pb}$ versus $^{206}\text{Pb}/^{204}\text{Pb}$. (b). $^{208}\text{Pb}/^{204}\text{Pb}$ versus $^{206}\text{Pb}/^{204}\text{Pb}$. (c). $^{206}\text{Pb}/^{207}\text{Pb}$ versus $^{208}\text{Pb}/^{207}\text{Pb}$. (d). $^{207}\text{Pb}/^{206}\text{Pb}$ versus $^{208}\text{Pb}/^{206}\text{Pb}$. The average crustal curve is from Stacey and Kramers (1975). (Data from Li 2011, 2018; Han 2013; Zheng et al. 2013; Hu 2015; Wang et al. 2016; Hao et al. 2016, 2020; Chen et al. 2017; Gao et al. 2017a, b, 2018; Liu et al. 2017; Zhang et al. 2017; Ma et al. 2018; Zhai et al. 2018; Liu et al. 2020; Zhao et al. 2020)

2. Descriptions of the Au-Ag Deposits

2.1. Sandaowanzi

Sandaowanzi produced 22 t of Au at an average grade of 13.9 g/t from quartz veins hosted in Early Cretaceous volcanic rocks (Tran et al. 2008; Zhao et al. 2010; Han et al. 2011; Yu et al. 2012; Xu et al. 2012; Liu et al. 2013; Zhai and Liu 2014; Gao et al. 2017a).

Volcanic rocks (Fig. 2a) consist of the Lower Cretaceous Longjiang (121.7 Ma) and Guanghua (122.0 Ma) Formations (Fm). The lower and upper parts of the Longjiang Formation contain eruptive- and lava flow-facies, respectively, with rock types comprising (brecciated) andesite and basaltic andesite. The Guanghua Formation contains lava flow-, pyroclastic-, sub-volcanic- and rare tuffaceous-facies, with rock types consisting of

volcanic breccias, agglomerates, rhyolite, perlite and dacite. Geochemically, these igneous rocks are calc-alkaline, enriched in LREEs, Pb, K, and U, and depleted in Nb, P, and Ti (Gao et al. 2017a).

Major structures include NW- and EW-trending faults, with the NW-trending normal faults being the major ore-hosting structures. The EW-trending faults are earlier than the volcanism and crosscut Jurassic intrusive rocks (Fig. 2a).

Igneous intrusions in the area include gray, medium-grained monzogranite of the Sandaowanzi (177.2 Ma; Gao et al. 2017a), fine-grained syenite (135.3 Ma; Liu et al. 2011), and dark gray, medium-grained granodiorite of the Sijianfangzi (118.7 Ma; Gao et al. 2017a). The Sijianfangzi granodiorite was emplaced under the Longjiang Formation andesite near the ore bodies. Dikes of diabase (116.6 Ma; Liu et al. 2011) crosscut the ore bodies.

Sandaowanzi contains Au- and Ag-telluride- bearing quartz veins. The ore bodies (40 in three belts) are hosted in the Lower Cretaceous Longjiang Formation (andesite and andesite breccia) along WNW-trending normal faults (Fig. 2a). Ore body II is the only current operating stope. The lenticular ore body is 212.6 m long and 0.81-14.3 m thick (averaging ~6 m). The ore body strikes 20–40°, dips 58–77°, and plunges to a depth of 520 m along the dip direction. The average grade of ore body II is 13.98 g/t Au.

Telluride minerals in the deposit include calaverite, krennerite, sylvanite, petzite, hessite, stützite, empressite, altaite and coloradoite, which coexist with chalcopyrite, sphalerite, tetrahedrite, galena, native gold and minor pyrite and bornite. Other silver-

bearing phases include argentite, pyrargyrite and kerargyrite. Petzite, sylvanite, calaverite and native gold assemblages generally occur in bonanza ore veins, and silver-bearing minerals occur in the upper parts of the ore bodies (Yu et al. 2012).

Alteration types include silicification and pyritization during stage I, silicification and sericitization in stage II, silicification, sericitization and carbonatization in stage III, and carbonatization, anhydritization, chloritization, and epidotization in stage IV. Plagioclase in wall rocks is mainly replaced by epidote, pyrite, calcite, sericite and chlorite. Euhedral laumontite occurs in stage I quartz vugs, whereas quartz, calcite and anhydrite commonly occur in stage IV veins. Pyrite, albite and chlorite alteration is widespread in wall rocks. Other alteration minerals include pyrophyllite and minor siderite.

Sericite from wall rocks at Sandaowanzi yielded $^{40}\text{Ar}/^{39}\text{Ar}$ plateau, isochron, and total gas dates that overlap within error, with a preferred age of 122.4 ± 3.9 Ma (Cheng 2017). Quartz veins and pyrite from wall rocks also produced an Rb-Sr isochron age of ~ 120 Ma (Zhai et al. 2015). These ages are similar to andesites of the host Longjiang Formation (121.7 Ma).

2.2. Yongxin

Yongxin produced 20 t Au at an average grade of 4.1 g/t from quartz-sericite-pyrite veins at the contact between late Carboniferous mylonite and Early Cretaceous volcanic rocks (Zhao et al. 2019, 2020).

Volcanic rocks consist of the Lower Cretaceous Longjiang and Guanghua Formations (Fig. 2b). The Longjiang Formation is located in the northern part of the district and is mainly composed of intermediate to acidic volcanic rocks (e.g., andesite, andesitic breccias, dacite, rhyolite, and rhyolitic tuff-breccias). The Guanghua Formation occurs in the southwestern part of the district and is mainly composed of rhyolite, dacite, and tuff. These two formations are calc-alkaline series (Fan et al. 2003; Ying et al. 2010; Li et al. 2013), and have been dated at 127–122 Ma (Li et al. 2013; Xu et al. 2013; Liu et al. 2014; Gao et al. 2017a; Li et al. 2020).

NE- to NEE-trending and NW-trending extensional faults occur at Yongxin (Fig. 2b). The NE- to NEE trending faults dip NWW at 25–40°, and the NW-trending faults dip SW at 15–30°. The NE-trending faults are the main ore-bearing structures and controlled the distribution of regional subvolcanic intrusive rocks. The NW-trending faults cross cut gold mineralization (Yuan et al. 2018).

Late Carboniferous syenogranite in the district has a zircon U–Pb age of 315.9 ± 1.6 Ma (Zhao et al. 2019). Granitic-dioritic mylonite has a protolith age of 310–290 Ma (Qu et al. 2015) and was deformed in the Jurassic (184–170 Ma; Zhao et al. 2015). Early Cretaceous diorite porphyry and granite porphyry dikes have NE- or NNE-strikes that are approximately parallel to the orebodies.

Two orebodies occur in echelon veins with lenticular-shapes that strike NE and dip NW at angles of 20–30°. Orebody I is approximately 375 m long and plunges 800 m deep, with thicknesses ranging from 6.8 to 73.4 m, and an average gold grade 3.92 g/t. Orebody

II is approximately parallel to orebody I, is 250 m long and plunges 330 m deep, with thicknesses ranging from 5.9 to 18.0 m, and an average gold grade of 3.55 g/t.

Ore minerals include pyrite, chalcopyrite, galena, sphalerite, native gold, Au-Ag-tellurides, and Bi-tellurides. Hydrothermal alteration is pervasive, consisting of quartz, sericite, chlorite, calcite, and pyrite; most of the ore is in the central zone of silicification (Yuan et al. 2018).

Pyrite from veins produced an Rb-Sr isochron age between 107–114 Ma (Zhao et al. 2019; Li et al. 2020) that is similar in age to the host Longjiang and Guanghua Formations.

2.3. Dong'an

Dong'an produced 24 t of Au at an average grade of 8.8 g/t from quartz-adularia veins hosted in Early Cretaceous volcanic rocks (Zhang et al. 2010).

Stratigraphy at Dong'an includes volcanic rocks of the Lower Cretaceous Guanghua Formation and Oligocene-Pliocene sandstone and conglomerate (Fig. 2c). The Guanghua Formation consists predominantly of rhyolitic lava and rhyolitic tuff with minor dacite that are underlain by an Early Jurassic coarse and fine-grained alkali feldspar granitic intrusion. The volcanic sequence and granitic intrusion are cut by rhyolite porphyry dikes.

The Dong'an area is cut by a series of tensile-shear NS-, NE- and NNE-trending faults (Fig. 2c). The 14 gold orebodies recognized in the mine are controlled by NS- and NE-striking faults that dip NW at 70° to 85°.

Eight of the orebodies are hosted in rhyolitic lavas, five are hosted in rhyolitic porphyry dykes, and one is hosted in Jurassic granite. Gold orebodies are commonly brecciated and the breccias are bounded by faults. The size of the gold veins varies considerably, from 50 to 800 m in length and from 1 to 7 m in thickness. They extend to depths of less than 400 m and have grades of 3–10 g/t Au. The largest vein is 770 m long, has a vertical extent of 358 m, has an average thickness of 6.7 m, and an average grade of 8.8 g/t Au and 75.8 g/t Ag.

Ore minerals are distributed as sparse disseminations, locally as dense disseminations, and as veinlets and stockwork veins. Pyrite, galena, chalcopyrite, sphalerite, hematite, argentite, petzite, hessite, altaite, native gold, electrum and native silver are present in the ores. Ore minerals are predominantly anhedral grains, although some display euhedral or subhedral textures. Quartz, adularia, chlorite and calcite are the most abundant gangue minerals, with fluorite in places.

The gold veins are enclosed by concentrically zoned alteration envelopes consisting of quartz, chalcedonic quartz, sericite, adularia, chlorite and pyrite.

The sericite $^{40}\text{Ar}/^{39}\text{Ar}$ date of 107.2 ± 0.6 Ma is within uncertainty of the zircon U-Pb date of 108.1 ± 2.4 Ma on rhyolite porphyry dikes (Zhang et al. 2010).

2.4. Tuanjiegou

Tuanjiegou produced 80 t Au at a grade of 4.0 g/t from quartz veins hosted in

Neoproterozoic metamorphic rocks and Early Cretaceous granodioritic porphyry (Sun et al. 2013b).

Stratigraphy in the Tuanjiegou district is composed of crystalline basement and volcanic cover rocks. Basement includes glaucophane chlorite schists, mica quartz schists and amphibolite schists of the Neoproterozoic Heilongjiang Group. (Fig. 2d; Wu et al. 2007). These rocks were affected by late Caledonian metamorphism at 437 ± 7 Ma (Xie et al. 2008). Volcanic cover consists of dacitic volcanic rocks of the Ningyuancun Formation (119 ± 1.4 Ma; Sun et al. 2013b) that may be equivalent to the Guanghua Formation (Qu 2008).

The NNE trending Tuanjiegou fault and WNW, NNW and NEE trending fractures controlled the distributions of subvolcanic intrusions and ore bodies in the district (Fig. 2d).

Intrusive rocks consist of a granodiorite porphyry stock and dykes (Sun et al. 2013b). The granodiorite porphyry contains plagioclase (20–25%) and quartz phenocrysts (5–10%), in a groundmass of plagioclase, alkali feldspar, quartz, and biotite. Magnetite, zircon, and apatite are the main accessory minerals. The EW-striking ore-bearing granodioritic porphyry stock is approximately 4 km in length and 0.75 km in width. LA-ICP-MS zircon U–Pb dates from the granodioritic porphyry range from 107 to 108 Ma (Wang et al. 2012), which are similar in age to the host volcanic rocks. A breccia belt that may be phreatomagmatic in origin occurs along a NWW splay of the Tuanjiegou fault at the contact between the granodiorite porphyry stock and Proterozoic metamorphic rocks of the Heilongjiang Group. The breccia belt has an irregular elliptical shape in plan, is

approximately 3 km in length, and 0.3 km in width. Breccia is rooted in granodioritic porphyry and has been traced vertically for less than 300 m.

Gold mineralization (about 83 ore bodies) occurs within breccia and in adjacent rocks of the Neoproterozoic Heilongjiang Group. Gold ore bodies occur along a NWW-trending fracture zone that dips northeast at 25°. The largest of the six major orebodies is approximately 925 m in length and 133 m in maximum thickness, with an average width of 46 m. The orebody extends to a depth of 450 m below the surface. This orebody accounts for about 59.4% of the total reserve, and has a maximum grade of 683 g/t Au (Li et al. 2008).

Orebodies contain chalcedony–pyrite–stibnite veins and minor calcite–pyrite veins. Pyrite and stibnite occur in chalcedony filled fractures in fragmented granodioritic porphyry. Most pyrite occurs as pentagonal dodecahedral crystals. Gold tellurides occur in fractured pyrite. Gangue minerals consist of quartz, chalcedony, calcite, illite and kaolinite. Banded and crustiform textures in the veins are typical. Bladed calcite is observed in the peripheral parts of the Tuanjiegou vein system and wall rocks.

Hydrothermal alteration is best developed in granodiorite and consists of quartz, sericite, calcite and kaolinite. An inner intense silicification-sericitization zone and an outer weak sericitization-carbonatization zone encompass the gold deposits.

Pyrite from veins produced an imprecise Rb-Sr isochron age about 114 Ma (Wang et al. 2014) that is similar to the host granodiorite (108 Ma).

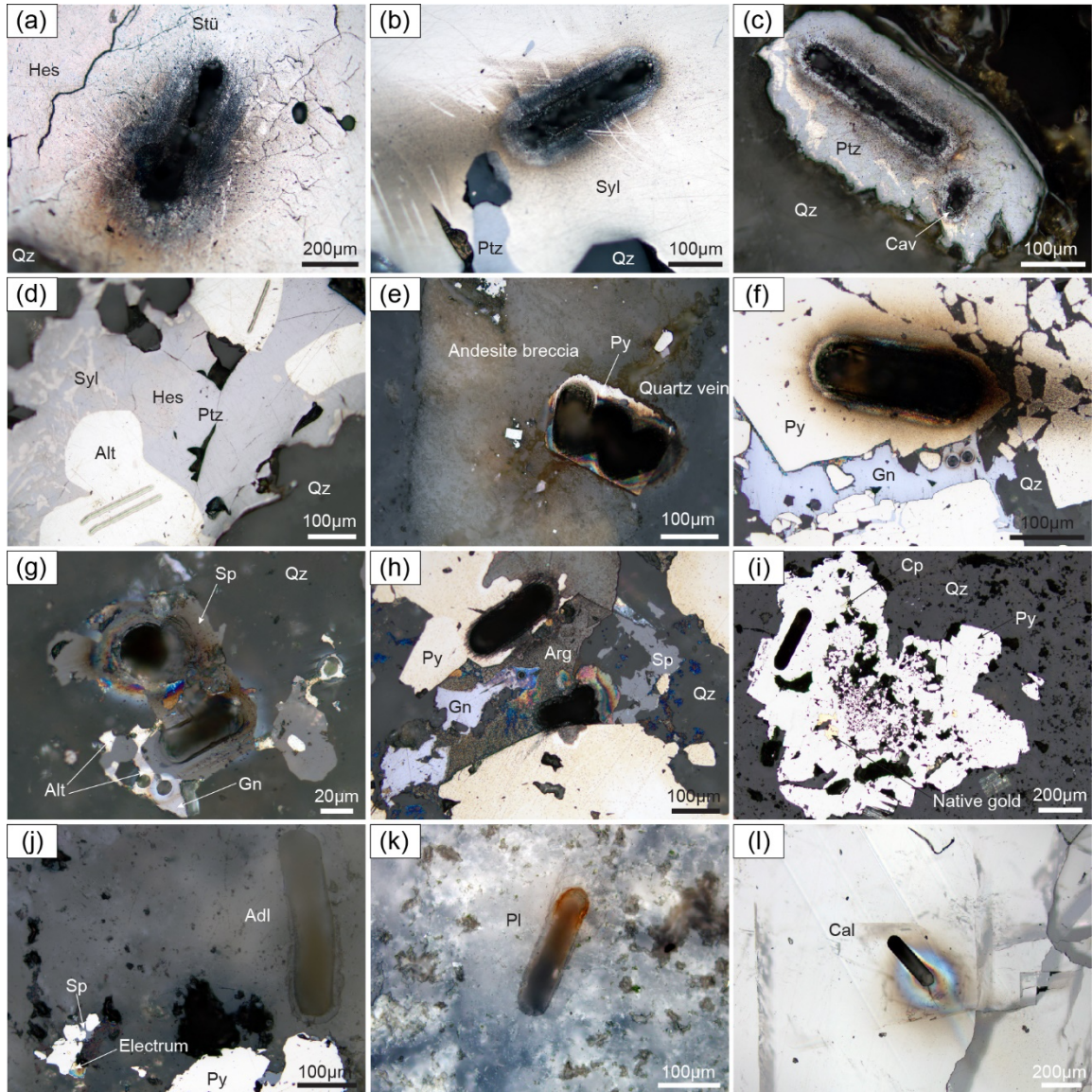


Fig. A3. Post laser ablation images of telluride, sulfide and gangue minerals analyzed for Pb isotope compositions using the femtosecond (*fs*) laser ablation multicollector inductively coupled plasma mass spectrometry (*fs* LA-MC-ICP-MS) with varying laser beam size (5–75 μm). Tracks from Sandaowanzi (a–e), Yongxin (f), Dong'an (g, h, and j), and Tuanjieou (i, k, and l). (a) Stützite coexisting with hessite in colloform quartz vein. (b) Sylvanite coexisting with petzite in colloform quartz vein. (c) Calaverite coexisting with petzite in colloform quartz vein. (d) Altaite coexisting with petzite, sylvanite and

hessite in colloform quartz vein. (e) Pyrite in andesite breccia replaced by quartz. (f) Altaite coexisting with galena and sphalerite in colloform quartz and adularia vein. (g) Galena replacing pyrite in quartz vein. (h) Argentite coexisting with galena, sphalerite and replacing pyrite in colloform quartz and adularia vein. (i) Pyrite associated with native gold in quartz vein. (j) Adularia associated with pyrite, sphalerite and electrum. (k) Plagioclase in granodiorite porphyry. (l) Crystalline calcite in colloform vein.

Abbreviation: Adl = adularia, Alt = altaite, Arg = argentite, Cal = calcite, Cav = calaverite, Cp = chalcopryite, Gn = galena, Hes = hessite, Pl = plagioclase, Ptz = petzite, Py = pyrite, Qz = quartz, Sp = sphalerite, Stü = stützite, Syl = sylvanite.

References

- Basu AR, Wang JW, Huang WK, Xie GH and Tatsumoto M (1991) Major element, REE, and Pb, Nd and Sr isotopic geochemistry of Cenozoic volcanic rocks of east-ern China: implications for their origin from suboceanic-type mantle reservoirs. *Earth and Planetary Science Letters* 105: 149-169.
- Chen X, Liu JJ, Zhang DH, Zhang QB, Yang SS, Li YC and Cao Q (2017) Re-Os dating of molybdenites and S-Pb isotopic characteristics of the Cuihongshan iron polymetallic deposit, Heilongjiang Province. *Acta Petrologica Sinica* 33: 529-544 (in Chinese with English abstract).
- Cheng L (2017) Ore genesis of the Sandaowanzi telluride-gold deposit in Heilongjiang

Province. MSc thesis, Jilin University, Changchun, China, pp 36-38 (in Chinese with English abstract).

Deng K, Li Q, Chen Y, Zhang C, Zhu X and Xu Q (2018) Geochronology, geochemistry and Sr-Nd-Pb-Hf isotopes of the Early Jurassic granodiorite from the Sankuanggou intrusion, Heilongjiang Province, Northeastern China: Petrogenesis and geodynamic implications. *Lithos* 296: 113-128.

Du Q (1988) *Geology of Duobaoshan porphyry copper deposit* Geological Publishing House, Beijing, pp 1-386 (in Chinese with English abstract).

Fan WM, Guo F, Wang YJ and Lin G (2003) Late Mesozoic calc-alkaline volcanism of post-orogenic extension in the northern Da Hinggan Mountains, northeastern China. *Journal of Volcanology and Geothermal Research* 121: 115-135.

Gao R, Xue C, Lv X, Zhao X, Yang Y and Li C (2017c) Genesis of the Zhengguang gold deposit in the Duobaoshan ore field, Heilongjiang Province, NE China: Constraints from geology, geochronology and S-Pb isotopic compositions. *Ore Geology Reviews* 84: 202-217.

Gao S, Xu H, Quan SL, Zang YQ and Wang T (2018) Geology, hydrothermal fluids, H-O-S-Pb isotopes, and Rb-Sr geochronology of the Daxintun orogenic gold deposit in Heilongjiang province, NE China. *Ore Geology Reviews* 92: 569-587.

Gao S, Xu H, Zang YQ, Yang LJ, Yang B and Wang T (2017a) Late Mesozoic magmatism and metallogeny in NE China: The Sandaowanzi-Beidagou example. *International Geology Review* 59: 1413-1438.

- Han S (2013) Magmatic fluids and gold mineralization of the late Mesozoic epithermal gold system in northern Lesser Xing'an Range, NE China. PhD thesis, Changchun, China, Jilin University, pp 47-50 (in Chinese with English abstract).
- Han SY, Zhai DG, Liu JJ, Lv J, Wu SH, and Yang LB (2011) Mineral assemblage of Sandaowanzi tellurium-gold deposit in Heilongjiang province and its genetic significance. *Mineral Deposits* 30: 855-866 (in Chinese with English abstract).
- Han Z (2004) The metallogenic series and evolution of metal and non-metal ore deposits in Heilongjiang Province. Geological Publishing House, Beijing, pp 1-241 (in Chinese with English abstract).
- Hao B, Deng J, Bagas L, Ge L, Nie F, Turner S and Qing M (2016) The Gaosongshan epithermal gold deposit in the Lesser Hinggan Range of the Heilongjiang Province, NE China: implications for Early Cretaceous mineralization. *Ore Geology Reviews* 73: 179-197.
- Hao Y, Ren Y, Yang Q, Sun Z, Ma Y and Lai K (2020) Fluid and ore sources of the tungsten mineralization in the Yangbishan iron-tungsten deposit, Heilongjiang Province, Northeastern China: Constraints from fluid inclusions, sulfide S-Pb isotopes and scheelite C-H-O-Sm-Nd isotopes. *Geological Journal* 55: 3957-3976.
- Hu XL (2015) Mineralization and magmatism of the porphyry Cu and Mo deposits in the northern Great Xing'an and Lesser Xing'an Ranges. PhD thesis, China University of Geosciences (Wuhan), pp 1-137 (in Chinese with English abstract).
- Li CL (2018) Gold metallogeny and prospecting in the Nenjiang-Heihe tectonic mélange

zone, Heilongjiang Province. PhD thesis, China University of Geosciences (Beijing), pp 1-182 (in Chinese with English abstract).

Li CL, Li L, Yuan MW, Alam M, Li SR, Santosh M, Deng CZ, Liu H and Xu GZ (2020)

Study on pyrite thermoelectricity, ore-forming fluids and H-O-Rb-Sr isotopes of the Yongxin gold deposit, Central Asian Orogenic Belt: Implications for ore genesis and exploration. *Ore Geology Reviews* 121: 103568.

Li D (2011) Ore genesis and exploration implication of the Sankuanggou copper polymetallic deposit in Heilongjiang Province, NE China. PhD thesis, China University of Geosciences (Beijing), pp 1-138 (in Chinese with English abstract).

Li JQ, Zhou K and Jin TH (2008) Geological characteristics and origin of Tuanjiegon gold deposit, Heilongjiang province. *Gold* 6: 19-24 (in Chinese with English abstract).

Li YF, Bian XF, Gao XY, Chen SW and Ding QH (2013) Laser $^{40}\text{Ar}/^{39}\text{Ar}$ chronology of the Mesozoic volcanic rocks from Longjiang basin in northern Da Hinggan Mountains. *Geological Bulletin of China* 33: 1212-1223 (in Chinese with English abstract).

Liu G, Lv XB, Chen C, Yang YS, Wang QJ and Sun YF (2014) Zircon U-Pb chronology and geochemistry of Mesozoic bimodal volcanic rocks from Nenjiang area in Da Hinggan mountains and their tectonic implications. *Acta Petrologica et Mineralogica* 33: 458-470 (in Chinese with English abstract).

Liu J, Li Y, Zhou ZH and Ouyang HG (2017) The Ordovician igneous rocks with high Sr/Y at the Tongshan porphyry copper deposit, satellite of the Duobaoshan deposit, and their metallogenic role. *Ore Geology Reviews* 86: 600-614.

- Liu Y, Chu X, Sun J, Han J, Ren L, Gu A, Zhao K and Zhao C (2020) Early Cretaceous bimodal magmatism related epithermal mineralization: A case study of the Gaosongshan gold deposit in the northern Lesser Xing'an Range, NE China. *Ore Geology Reviews* 21: 103563.
- Ma YP, Ren YS, Hao YJ, Lai K, Zhao HL and Liu J (2018) Ore genesis and material source of scheelite mineralization of Yangbishan iron-tungsten deposit in Heilongjiang Province, NE China. *Journal Jilin University Earth Science Edition* 48: 105-117 (in Chinese with English abstract).
- Qu GS (2008) *Lithostratigraphy of Heilongjiang province, China*: Wuhan, China University of Geosciences Press, pp 1-301 (in Chinese).
- Qu H, Li CL and Yang FS (2015) Zircon U-Pb ages, geochemical characteristics and their geological implication of granitic complex in Huolongmen area, northwestern Xiao Hinggan mountains. *Global Geology* 34: 34-43 (in Chinese with English abstract).
- Rasskazov SV, Chuvashova IS, Liu Y, Meng F, Yasnygina TA, Fefelov NN and Saranina EV (2011) Proportions of lithospheric and asthenospheric components in Late Cenozoic K and K-Na lavas in Heilongjiang Province, Northeastern China. *Petrology* 19: 568-600.
- Stacey JS and Kramers JD (1975) Approximation of terrestrial lead isotope evolution by a two-stage model. *Earth and Planetary Science Letters* 26: 207-221.
- Sun JG, Han SJ, Zhang Y, Xing SW and Bai LA (2013b) Diagenesis and metallogenetic mechanisms of the Tuanjiegou gold deposit from the Lesser Xing'an Range, NE China:

Zircon U–Pb geochronology and Lu–Hf isotopic constraints. *Journal of Asian Earth Sciences* 62: 373-388.

Tran M, Liu JL, Hu JJ, Zou YX and Zhang HY (2008) Discovery and geological significance of Sandaowanzi telluride type gold deposit in the northern Daxing'anling, Heilongjiang, China. *Geological Bulletin of China* 27: 548-587 (in Chinese with English abstract).

Wang PJ, Chen F, Chen SM, Siebel W and Satir M (2006b) Geochemical and Nd-Sr-Pb isotopic composition of Mesozoic volcanic rocks in the Songliao basin, NE China: *Geochemical Journal* 40: 149-159.

Wang XJ, Chen LH, Hofmann AW, Mao FG, Liu JQ, Zhong Y, Xie LW and Yang YH (2017) Mantle transition zone-derived EM1 component beneath NE China: Geochemical evidence from Cenozoic potassic basalts. *Earth and Planetary Science Letters* 465: 16-28.

Wang Y, Zeng Q, Zhou L, Chu S and Guo Y (2016) The sources of ore-forming material in the low-sulfidation epithermal Wulaga gold deposit, NE China: Constraints from S, Pb isotopes and REE pattern. *Ore Geology Reviews* 76: 140-151.

Wang YB, Liu JM, Sun SK, Li Y, Li FY and Hu HT (2012) Zircon U-Pb geochronology, petrogenesis and geological implication of ore-bearing granodiorite porphyry in the Wulaga gold deposit, Heilongjiang Province. *Acta Petrologica Sinica* 28: 557-570.

Wang YB, Zeng QD and Liu JM (2014) Rb–Sr dating of gold-bearing pyrites from Wulaga gold deposit and its geological significance. *Resource Geology* 64: 262-270.

- Wu FY, Yang JH, Lo CH, Wilde SA, Sun DY and Jahn BM (2007) The Heilongjiang Group: a Jurassic accretionary complex in the Jiamusi Massif at the western Pacific margin of northeastern China. *Island Arc* 16: 156-172.
- Xie HQ, Zhang FQ, Miao LC, Chen FK and Liu DY (2008) Zircon SHRIMP U–Pb dating of the amphibolite from “Heilongjiang Group” and the granite in Mudanjiang area, NE China, and its geological significance. *Acta Petrologica Sinica* 24: 1237-1250 (in Chinese with English abstract).
- Xu H, Yu YX, Wu XK, Yang LJ, Tian Z, Gao S and Wang QS (2012) Intergrowth texture in Au-Ag-Te minerals from Sandaowanzi gold deposit, Heilongjiang Province: Implications for ore-forming environment. *Chinese Science Bulletin* 57: 2778-2786.
- Xu WL, Pei FP, Wang F, Meng E, Ji WQ, Yang DB and Wang W (2013) Spatial-Temporal relationships of Mesozoic volcanic rocks in NE China: Constraints on tectonic overprinting and transformations between multiple tectonic regimes. *Journal of Asian Earth Sciences* 74: 167-193.
- Ying JF, Zhou XH, Zhang LC and Wang F (2010) Geochronological framework of Mesozoic volcanic rocks in the Great Xing'an Range, NE China, and their geodynamic implications. *Journal of Asian Earth Sciences* 39: 786-793.
- Yu YX, Xu H, Wu XK, Yang LJ, Tian Z, Gao S and Wang QS (2012) Characteristics of the Au-Ag-Te minerals and its ore-forming fluids in Sandaowanzi gold deposit, Heilongjiang Province. *Acta Petrologica Sinica* 28: 345-356 (in Chinese with English abstract).

- Yuan MW, Li SR, Li CL, Santosh M, Alam M and Zeng YJ (2018) Geochemical and isotopic composition of auriferous pyrite from the Yongxin gold deposit, Central Asian Orogenic Belt: Implication for ore genesis. *Ore Geology Reviews* 93: 255-267.
- Zhai DG, Williams-Jones AE, Liu JJ, Tombros SF and Cook NJ (2018) Mineralogical, fluid inclusion and multiple isotope (H-O-S-Pb) constraints on the genesis of the Sandaowanzi epithermal Au-Ag-Te deposit, NE China. *Economic Geology* 113: 1359-1382.
- Zhai DG and Liu JJ (2014) Gold-telluride-sulfide association in the Sandaowanzi epithermal Au-Ag-Te deposit, NE China: Implications for phase equilibrium and physicochemical conditions. *Mineralogy and Petrology* 108: 853-871.
- Zhai DG, Liu JJ, Edward MR and Wang JP (2015) Geochronological and He-Ar-S isotopic constraints on the origin of the Sandaowanzi gold-telluride deposit, northeastern China. *Lithos* 212: 338-352.
- Zhang C, Wang E, Bi Z, Han R, Shao J, Liu B, Chen J and Zeng N (2019) Geochronology and isotope geochemistry studies of an epithermal gold deposit in the northern Lesser Khingan Range, NE China: The Gaosongshan example. *Ore Geology Reviews* 105: 356-374.
- Zhang LL, Liu C, Zhou S, Sun K, Qiu RZ and Feng Y (2014) Characteristics of ore-bearing granites and ore-forming age of the Huojihe molybdenum deposit in Lesser Xing'an Range. *Acta Petrologica Sinica* 30: 3419-3431 (in Chinese with English abstract).
- Zhang M, Suddary P, Thompson RN, Thirlwall MF and Menzies MA (1995) Potassic

volcanic rocks in NE China: Geochemical constraints on mantle source and magma genesis. *Journal Petrology* 36: 1275-1303.

Zhang YM, Gu XX, Liu RP, Sun X, Li XL and Zheng L (2017) Geology, geochronology and geochemistry of the Gaogangshan Mo deposit: A newly discovered Permo-Triassic collision-type Mo mineralization in the Lesser Xing'an Range, NE China. *Ore Geology Reviews* 81: 672-688.

Zhang Z, Mao J, Wang Y, Pirajno F, Liu J and Zhao Z (2010) Geochemistry and geochronology of the volcanic rocks associated with the Dong'an adularia-sericite epithermal gold deposit, Lesser Hinggan Range, Heilongjiang province, NE China: Constraints on the metallogensis. *Ore Geology Reviews* 37: 158-174.

Zhao SJ, Liu JL, Bai XD, Zhao HB, Lu J, Chen Y and Tran MD (2010) Fluid inclusions and sulfur isotopes of Sandaowanzi gold telluride deposit, Heilongjiang Province. *Mineral Deposits* 29: 476-488 (in Chinese with English abstract).

Zhao YD, Che JY, Li SC, Wang KL, Zhao J, Wu DT, Xu FM and Sun QS (2015) Late Jurassic rapakivi granite and its geological implication of the northeast Great Xing'an Range, China: Chinese Mineral Geochemistry Society 15th Annual Conference Abstract Book, v 1 (in Chinese).

Zhao Z, Sun J, Li G, Xu W, Lv C, Guo Y, Liu J and Zhang X (2020) Zircon U–Pb geochronology and Sr–Nd–Pb–Hf isotopic constraints on the timing and origin of the Early Cretaceous igneous rocks in the Yongxin gold deposit in the Lesser Xing'an Range, NE China. *Geological Journal* 55: 2684-2703.

- Zhao ZH, Sun JG, Li GH, Xu WX, Lv CL, Wu S, Guo Y, Ren L and Hu ZX (2019) Age of the Yongxin Au deposit in the Lesser Xing'an Range: Implications for an Early Cretaceous geodynamic setting for gold mineralization in NE China. *Geological Journal* 54: 2525-2544.
- Zheng L, Gu XX, Zhang YM and Liu RP (2013) Isotopic geochemistry and its implication to the genesis of Gaosongshan epithermal gold deposit in Heilongjiang Province, China. *Acta Mineralogica Sinica* 33: 101-109 (in Chinese with English abstract).
- Zheng Q (2012) Geological characteristics and ore genesis of Zhengguang gold deposit in Heihe area, Heilongjiang Province MSc thesis, Jilin University, Changchun, China, pp 1-45 (in Chinese with English abstract).
- Zou HB, Reid MR, Liu YS, Yao YP, Xu XS and Fan QC (2003) Constraints on the origin of historic potassic basalts from northeast China by U–Th disequilibrium data. *Chemical Geology* 200: 189-201.